ELSEVIER

Contents lists available at ScienceDirect

Proceedings of the Combustion Institute

journal homepage: www.elsevier.com/locate/proci



Stabilisation limits of turbulent premixed flames by nanosecond repetitively pulsed discharges



Department of Engineering, University of Cambridge, Cambridge CB2 1PZ, United Kingdom

ARTICLE INFO

Keywords: Flame stabilisation Nanosecond repetitively pulsed discharges Plasma-assisted combustion Spark ignition

ABSTRACT

The mechanism of flame stabilisation using nanosecond repetitively pulsed (NRP) plasma discharges in a turbulent, premixed methane-air flame at high velocities was investigated, focusing on the lean extinction limits. In contrast to the majority of the existing studies that considered NRP discharges as an assistance to conventional stabilisers, here, no other flame-holding method is used. High-speed (10 kHz) OH* chemiluminescence showed that the plasma discharges produce individual OH*-pockets that merge together at a high enough frequency to form a continuous flame sheet. Increasing the discharge repetition frequency from 5 kHz to 10 kHz improves flame stability, but no change in flame structure and stability was observed when the frequency was increased beyond 10 kHz. Change in the plasma energy level in the range studied had little effect on the flame structure. The lean extinction limit was quantified at various flow velocities, equivalence ratios, discharge frequencies and energy levels. It was observed that the trend of the extinction equivalence ratio with bulk velocity was similar to that of a conventional bluff body stabilised flame and that plasma-only stabilised flame was equally effective at certain operating conditions. An effort to correlate the stabilisation limits by a conventional Damköhler number Da* was made but was not satisfactory due to the presence of a characteristic flameholder lengthscale present in the Da* expression. A modified Da* was proposed to take the spark frequency effects into account, but this was not successful either. In contrast, the spread of the extinction data was smaller when a critical Karlovitz number was used, hence offering a way to extrapolate the present data to other conditions. The experiments demonstrate that NRP discharges can be used as an alternative stabilisation method for high-speed turbulent premixed flames.

1. Introduction

Lean flame stabilisation is of paramount importance for combustion in gas turbines as they facilitate low NO_{X} and soot emissions. Traditional methods of lean flame stabilisation include the utilisation of a flame holder such as a bluff body, swirler, or steps and angles in combustor walls [1–3]. The recirculation/wake regions produced by these flame holders allow the recirculation of hot products, which then mix with the incoming reactants to stabilise the flame. Recently, plasma discharges have received interest in extending the stability limits of combustors comprising a conventional stabiliser [4–6], hence establishing a large body of work described by the phrase plasma-assisted combustion. Significant progress has been made in the last decade towards understanding the effect of non-equilibrium plasma discharge on flames, including studying plasma–chemistry interactions, energy redistribution in discharge plasma, and non-equilibrium initiation of combustion [7–10].

Among the different non-equilibrium plasma techniques, the method that is attracting attention is the nanosecond repetitively pulsed $% \left\{ 1\right\} =\left\{ 1\right$

(NRP) discharges due to its ability to generate high electron temperature and density. In NRP discharges, high voltage electric pulses are applied at a high repetition rate, typically 5 to 100 kHz [11], with the resulting spark discharges lasting a few nanoseconds. These discharges in a fuel–air mixture can produce thermal, chemical and hydrodynamic effects [12–14] that can be favourable for combustion.

A significant improvement in lean blowout (LBO) limits of spray flames was observed in [15] on a swirl combustor with NRP discharges. The authors found that by the placement of electrodes in the outer recirculation zone, the stability limits of spray flames can be extended. Recently, Blanchard et al. [16] studied the effect of plasma on the LBO limit on a two-stage swirl combustor with methane as fuel. The authors found that NRP discharges can stabilise the flame at ultralean conditions down to an equivalence ratio of 0.16 for flame powers up to $100\,\mathrm{kW}$. The other major observation in this study is the lower amount of NO_{x} emitted by plasma-assisted flames compared to the leanest stable flame without plasma, which is a contrast from [17].

E-mail address: pr516@cam.ac.uk (P. Rajendram Soundararajan).

https://doi.org/10.1016/j.proci.2024.105722

Corresponding author.

Further, the authors also indicate that flame stabilisation at lower plasma power and pollutant emissions can be achieved by tuning the repetition frequency instead of continuous application of plasma. Some of the critical factors in achieving improved flame stability include the location of the discharge [6,15] and repetition rates [18].

Numerical tools are also being increasingly used to study plasma-assisted combustion. One such study to identify the mechanism of stabilisation by NRP discharges on a premixed bluff-body stabilised flame was conducted by Yacine & Fiorina [19]. The authors found that improved flame stability with plasma occurs due to the dissociation of the burnt gas species, which are convected to the flame front by the flow, where they are consumed with increased chemical reactivity, leading to a local increase in heat release rate. In addition to extending the stability limits, non-equilibrium plasma is also used to suppress combustion instabilities [20–22] and reduce ignition delay time [23–25].

In the aforementioned studies, the primary source of stabilisation is the recirculation zone, created by a bluff body, swirl, or both, and the plasma source is used to improve the extinction limits or dynamic response of the flame. However, the presence of a flame stabiliser in the flow path imposes a pressure drop, which may not be desirable. One then naturally questions whether it is possible to stabilise a flame solely using plasma discharges, thus eliminating the need for a conventional stabiliser. Kong et al. [26] carried out such a study on an open jet flame using filamentary plasma discharges to understand the mechanism of flame stabilisation. The authors observed a spatial separation between the plasma column and flame front, indicating that the impact of plasma on the flame is through thermal effects. Similar studies have been carried out experimentally by Lefkowitz and Ombrello [27], who found that by suitably modifying the inter-pulse time, the discharge kernels can merge to form a freely propagating flame. This configuration was numerically investigated by Yacine and Fiorina [28], who also proposed a model based on dimensional analysis to identify the different flame regimes. More recently, Patel et al. [29] observed that at a higher pulse repetition rate, strong pulse-to-pulse coupling enables successful flame ignition. However, these works were carried out at relatively low flow velocities (less than 10 m/s), typically in the laminar flow regime and focused primarily on flame ignition with plasma discharges. In contrast, the present study attempts to explore flame stabilisation in highly turbulent flows, with the aim of replacing conventional recirculation zone stabilisers with NRP discharges.

This paper is organised as follows. The description of the experimental setup and measurement techniques is provided in Section 2. The results are firstly discussed using high-speed chemiluminescence imaging in Section 3.1. The stability limits of the turbulent flames with plasma discharges are explored in Section 3.2 and compared against conventional bluff body stabilised flames. Finally, the mechanism of stabilisation with plasma discharges is discussed in Section 4 and the conclusions of this study are drawn in Section 5.

2. Experimental methods

2.1. Burner configuration

The burner comprises a square-cross-section duct with dimensions $25~\mathrm{mm} \times 25~\mathrm{mm}$. Methane is mixed with air ahead of the plenum formed by a 300 mm-long tube leading to the combustion chamber. The chamber is 50 mm long and enclosed by quartz plates on four sides to provide optical access. The schematic of the experimental setup, along with important dimensions, is shown in Fig. 1(a). The air and the fuel mass flow rates are controlled by Alicat mass flow controllers, having an accuracy of $\pm 1.5\%$. Plasma discharges are produced between two tungsten electrodes of $d_e=2~\mathrm{mm}$ diameter, and oriented perpendicular to the flow. The electrodes are separated by a distance of $\delta_e=1.65~\mathrm{mm}$. The supply to the electrodes is provided by a custom-made high-voltage plasma generator unit that can be operated at different

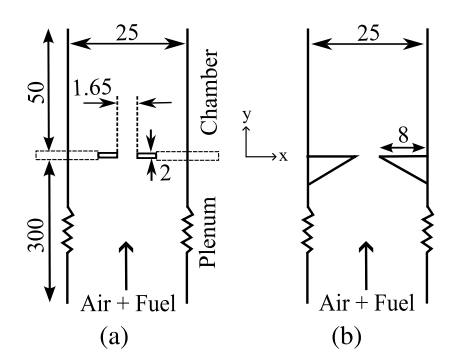


Fig. 1. (a) Burner schematic showing the critical dimensions and electrode location. (b) Step bluff body configuration used for comparison with plasma-stabilised flames. All dimensions are in mm and are not to scale.

repetition frequencies and energy levels. The generator features a pulse rise time of 4 ns with a pulse width of 10 ns. In this study, the NRP discharge unit is operated at five frequency levels of f=5,10,15,20 and 30 kHz and at two energy levels. The chamber has no other stabiliser, and the premixed flame is stabilised solely using NRP discharges. All experiments are conducted at velocities exceeding 23 m/s to prevent any stabilisation in the wake generated behind the electrodes. To verify that the flames are solely stabilised by the NRP discharges, under stable flame conditions before each measurement, the NRP discharge is deactivated to observe whether the flame would establish itself within the wake of the electrodes. The complete experimental setup is contained within a Faraday cage to avoid electromagnetic interference produced by the spark.

In addition to the above configuration, a V-gutter (step bluff body) is also used to compare the stabilisation characteristics with the plasma-stabilised configuration. In this arrangement, the electrodes are replaced by step bluff bodies with dimensions $8\,\mathrm{mm}\times 8\,\mathrm{mm}$ when viewed from the top and featuring a 45° angle (shown in Fig. 1(b)) in the direction facing the flow, resulting in a blockage ratio (defined as bluff body area over duct area) of approximately 40%. The premixed fuel—air mixture is ignited using a hand-held torch in the bluff body configuration. These experiments are only performed to compare the extinction limits of plasma-only vs. a conventional system.

2.2. Measurements

The voltage and current characteristics of the nanosecond generator unit are recorded using a *PVM-1* high-voltage probe and *Pearson 7713-03* current probe, respectively. From this, the plasma energy is calculated using the equation:

$$\epsilon = \int v(t)i(t)dt \tag{1}$$

where v(t) and i(t) correspond to the measured time traces of voltage and current. From Fig. 2, it can be seen that the energy deposited at the two levels considered in this study is ≈ 2.8 mJ and ≈ 3.2 mJ. It can also be seen from the figure that the energy rises until about 300 ns and stabilises beyond that. One can observe from the corresponding voltage and current waveforms (not shown here) that the pulse rises until around 12 ns, followed by reflections in the system, which manifests as an increase in pulse energy until the oscillations diminish. This is typically seen in several other plasma systems used for similar purposes in the literature (see, for example, Fig. 2 in [27] and Fig. 3 in [15]).

A *Photron SA 1.1* high-speed camera fitted with a *Lavision IRO* intensifier unit (spectral range 190–800 nm) is used to capture the chemiluminescence emitted by the flame. The measurements are carried out at $10\,\mathrm{kHz}$ with the intensifier gated at 90 μs for a total acquisition time of 1.2 s. The camera-intensifier unit is fitted with a *CERCO* $100\,\mathrm{mm}$ UV-lens comprising a narrow bandpass filter of $310\,\pm$

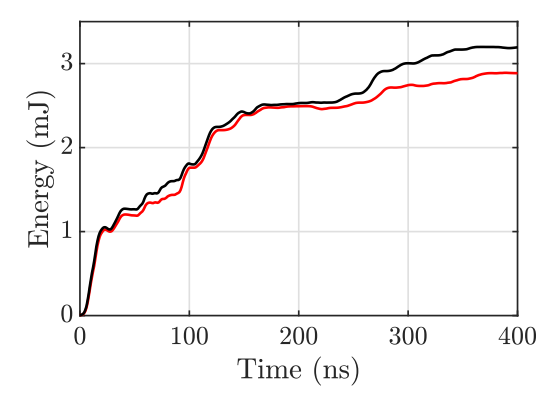


Fig. 2. Calculated energy from voltage and current traces at two energy levels of the plasma generator.

10 nm (Edmund optics) to capture the light intensity emissions corresponding to the OH* radical from the flame. The images are captured at different repetition frequencies, energy levels and bulk velocities in order to identify the different flame regimes. In the next step, the lean extinction limit of the plasma-stabilised flame is evaluated at different bulk flow velocities in the range between 18 m/s to 35 m/s. The extinction limits of the bluff body configuration are also determined in a similar way and compared against the performance of the plasma-stabilised flame.

3. Results

3.1. High-speed chemiluminescence

Fig. 3 shows the effect of bulk velocity on the flame stabilisation at a NRP frequency of 5 kHz and a pulse energy of 3.2 mJ. The four images (in every row) shown at each operating point correspond to the different frames acquired at 10 kHz for a time duration of 1.2 s. The velocity was increased from 23 m/s to 38 m/s in steps of 5 m/s while maintaining a constant equivalence ratio of $\phi = 0.9$. The fuelair mixture ignited by the NRP discharge resulted in the formation of OH*-pockets (flame kernel), which were convected downstream by the flow. The OH*-pockets were observed to increase in size as they moved downstream (see red circle in Fig. 3). At 23 m/s, the individual OH*pockets were observed to merge between 5-10 mm from the chamber inlet (marked by a red circle in Fig. 3), leading to the formation of a continuous stable flame as marked by red rectangle beyond 15 mm. As the velocity was increased to 28 m/s, the OH*-pockets propagated with the flow and were observed to merge in the region of $5-20\,\mathrm{mm}$ (marked by the red rectangle in the second row), leading to the formation of a stable flame in the downstream regions beyond 25 mm (out of the field of view of the camera). The individual OH*-pockets were observed to be 3 to 5 mm in diameter. At 33 m/s, the OH*-pockets were observed to propagate with the flow but were, however, extinguished in the downstream regions (marked by white circles). As the u_h was further increased to 38 m/s, the individual OH*-pockets were observed to disappear as soon as they were formed by the individual NRP discharge events (see green ellipse and rectangle).

Fig. 4 illustrates the flame structure at an NRP frequency of $10\,\mathrm{kHz}$ and a pulse energy of $3.2\,\mathrm{mJ}$. An increase in OH* intensity was observed with increasing frequency, which is due to the increase in total energy input to the system. The OH*-pockets were observed to merge at the exit plane of the burner, leading to a stable flame in the downstream regions at $u_b = 23$ and $28\,\mathrm{m/s}$. At $33\,\mathrm{m/s}$, a decrease in OH* intensity is observed between $10{\text -}25\,\mathrm{mm}$, indicating that the flame is close to extinction. On increasing the velocity further to $38\,\mathrm{m/s}$, a continuous stream of OH*-pockets is observed at the exit plane. However, these

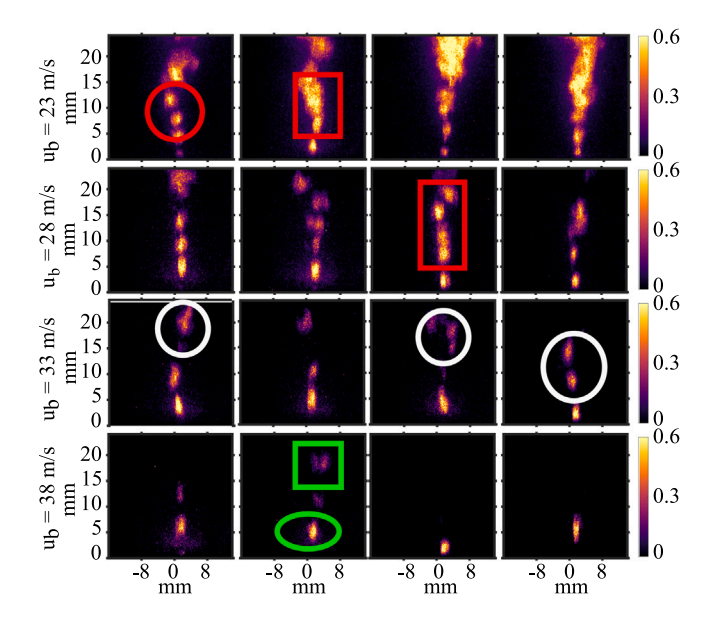


Fig. 3. OH* chemiluminescence at an NRP discharge frequency of $f = 5 \,\mathrm{kHz}$ and pulse energy of $e = 3.2 \,\mathrm{mJ}$ for a range of bulk velocities (u_b) at an equivalence ratio of $\phi = 0.9$. The intensity is normalised by its maximum in each image. (For interpretation of the references to colour in this figure legend, the reader is referred to the web version of this article.)

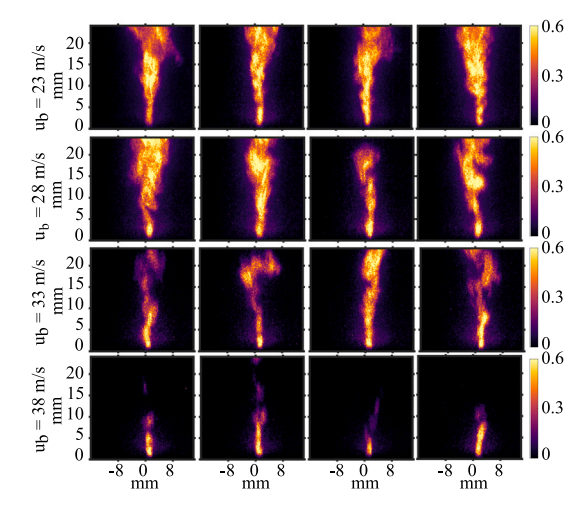


Fig. 4. OH* chemiluminescence at an NRP discharge frequency of $f=10\,\mathrm{kHz}$ and pulse energy of $\epsilon=3.2\,\mathrm{mJ}$ for a range of bulk velocities (u_b) at an equivalence ratio of $\phi=0.9$. The intensity is normalised by its maximum in each image.

pockets are observed to disappear beyond $10\,\mathrm{mm}$. A video of the high-speed images at some of these operating conditions is provided in the Supplementary Material.

Increasing the frequency of NRP discharges to $15\,\mathrm{kHz}$ at the same energy $3.2\,\mathrm{mJ}$ resulted in no change in flame structure at lower bulk velocities (23 and 28 m/s), when the OH*-pockets merge, as shown in Fig. 5 (first and second row). However, differences can be observed when the velocity is increased (at 33 and 38 m/s shown in third and fourth row) when the flame is closer to extinction. Increasing the NRP frequency from $10\,\mathrm{kHz}$ to $15\,\mathrm{kHz}$ showed no effect on the maximum velocity at which the flame can be stabilised. The OH*-pockets were observed to extinguish after detaching from the electrodes at a velocity of $38\,\mathrm{m/s}$. The velocity at which the OH*-pockets disappear in the downstream region and do not result in a stable flame is defined as the critical velocity (u_{cric}).

Fig. 6 illustrates the effect of pulse energy at a constant repetition frequency (10 kHz) on the flame structure. The increased pulse energy

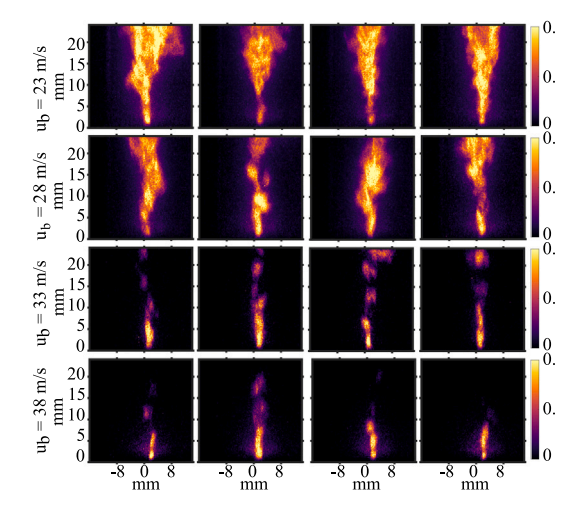


Fig. 5. OH* chemiluminescence at an NRP discharge frequency of $f = 15\,\mathrm{kHz}$ and pulse energy of $\epsilon = 3.2\,\mathrm{mJ}$ for a range of bulk velocities (u_b) at an equivalence ratio of $\phi = 0.9$. The intensity is normalised by its maximum in each image.

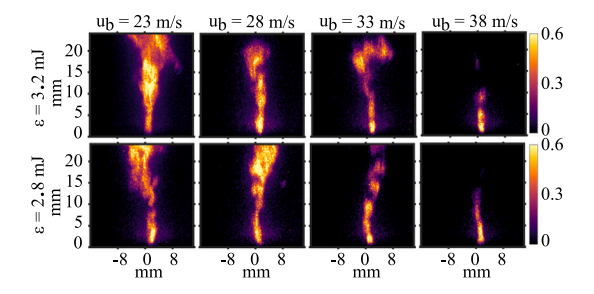


Fig. 6. OH* chemiluminescence images at an NRP discharge frequency of $f=10\,\mathrm{kHz}$ and comparison of the pulse energy at $\epsilon=3.2\,\mathrm{mJ}$ and $\epsilon=2.8\,\mathrm{mJ}$ for a range of bulk velocities (u_b) at an equivalence ratio of $\phi=0.9$. The intensity is normalised by its maximum in each image.

did not show any effect on the flame structure or dynamics as well as on $u_{cric}.$

3.2. Lean extinction limits

From the high-speed OH* chemiluminescence images, three distinct flame regimes were observed: (a) stable flame far from extinction (see Figs. 3, 4, 5 at 23 m/s) (b) unstable flame near extinction (see Figs. 3, 4, 5 at 33 m/s), and (c) flame unable to propagate after ignition (OH*-pockets disappearing after ignition, see Figs. 3, 4, 5 at 38 m/s).

The lean extinction limit was quantified at different NRP frequencies and energy levels. The measurements were performed at a constant air flow rate, and the fuel flow rate was gradually varied by changing the equivalence ratio at the rate of 0.02 per 20 s. Extinction is determined based on the visual structure of the flame and whether the spark is capable of igniting the fuel–air mixture continuously. The experiments were also carried out to determine the extinction limit of a flame established by a conventional flame stabiliser, a bluff body in this case (see Fig. 1, right), and compared with the plasma-stabilised case. For the bluff body configuration, the flame is considered to be extinct when the bluff body cannot hold a flame (i.e., zero chemiluminescence), as in the case of a typical lean blow-off determination (see [1], for example).

Fig. 7 presents the lean extinction equivalence ratio ϕ_{extinct} as a function of u_b at different plasma repetition frequency f and energy ϵ . It is observed that the extinction equivalence ratio increases with an increase in bulk velocity, as for the flame stabilised by the conventional bluff body (also noted in [1]). The flames at 10, 15, 20, and 30 kHz blow off at a lower equivalence ratio than 5 kHz (blue symbols) at both

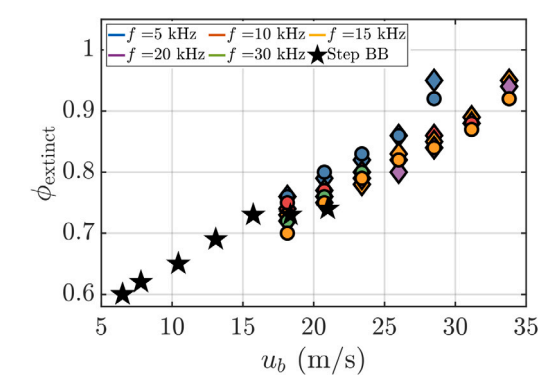


Fig. 7. Lean extinction limit $\phi_{\rm extinct}$ as a function of bulk velocity u_b at different repetition frequencies f. The diamonds correspond to a pulse energy of $\epsilon=2.9\,{\rm mJ}$ and the circles correspond to a pulse energy of $\epsilon=3.2\,{\rm mJ}$. The results are also compared against a step bluff body (BB) stabiliser shown with black pentagrams. (For interpretation of the references to colour in this figure legend, the reader is referred to the web version of this article.)

energy levels. Thus, an increase in frequency from 5 kHz (blue symbols) to 10 kHz (orange symbols) has an effect on lean extinction limits, but increasing frequency further has little to no effect on lean extinction limits. Additionally, no effect was observed on the lean extinction limits with increased pulse energy. The reviewers of this article raised a question on whether a 14% change in the energy level is sufficient to arrive at this conclusion. Experiments were also conducted at an energy level of 5 mJ, which corroborates this observation. The comparison between the three energy levels on lean extinction limits is shown in the Supplementary Material at a repetition frequency of 15 kHz. It is interesting to note that a spark frequency greater than 10 kHz is as effective as a conventional burner stabiliser (black pentagrams) at certain operating points. For the step bluff body case, the bulk velocity was calculated after accounting for the 40% blockage it imposes on the flow. In spite of this, the reported bulk velocities are lower for the bluff body configuration as the edge velocities are comparatively higher (40-70 m/s), and consequently, the bluff body was unable to stabilise the flame in the higher bulk velocity range of plasma-stabilised cases.

4. Discussion

From Section 3.1, it is seen that the NRP discharge frequency less than 10 kHz plays a crucial role in determining the stability limits of the combustor (see Figs. 3-5), thus indicating that the characteristic time scales are the chemical time scale and an OH*-pocket convection time scale. Moreover, at critical velocity, $u_{cric} = 38 \text{ m/s}$, the individual OH*-pockets were observed to disappear before propagating. As an OH*-pocket is produced by a spark discharge, it is convected downstream by the bulk velocity and successive OH*-pockets are produced at the rate of the NRP frequency. A schematic of flame stabilisation with plasma is shown in Fig. 8. The inter-OH*-pockets distance $L_{\rm int}$ can be defined as $L_{\text{int}} = u_b/f$, where u_b is the bulk flow velocity, and f is the plasma repetition frequency. In Fig. 8(a), the higher bulk velocity does not allow the merging of the successive OH*-pockets formed by the NRP discharges. However, when the bulk velocity is smaller, the successive OH*-pockets merge, as shown in Fig. 8(b), giving the condition $L_{\rm int}$ is equal to or less than the individual OH*pocket diameter d_k . If one increases the repetition frequency, as shown in Fig. 8(c), OH*-pockets are formed more rapidly, allowing flame stabilisation at a higher bulk velocity. Similar observations were made by Ref. [27] for the velocity range of 2-10 m/s. The authors identified three regimes based on the inter-pulse time, namely a fully-coupled regime where the kernels develop into a freely propagating flame, a partially-coupled regime where kernels interact but do not develop into a fully coupled regime, and a decoupled regime where the kernels do

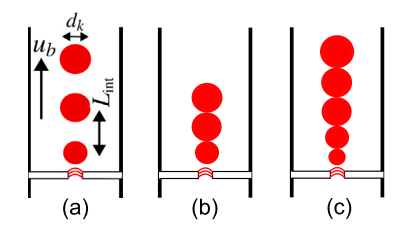


Fig. 8. Schematic showing the mechanism of flame stabilisation with NRP discharges. (a) An unstable flame with individual flame kernels unable to merge. (b) A stable flame with merged flame kernels formed due to a decrease in bulk flow velocity. (c) A stable flame with merged flame kernels formed due to an increase in plasma repetition frequency.

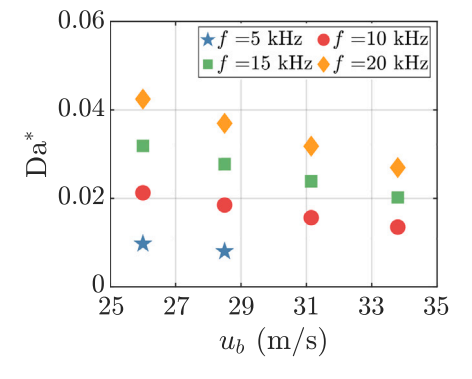


Fig. 9. Evolution of the critical Damköhler number Da^* with bulk velocity u_b and repetition frequency f. (For interpretation of the references to colour in this figure legend, the reader is referred to the web version of this article.)

Table 1
Residence time for the OH*-pockets.

residence time for the off poetics.			
Diameter of	u_b (m/s)	Residence	Frequency
OH*-pockets		time (ms)	(kHz)
(mm)			
3.0	23	0.13	7.7
3.0	28	0.11	9.3
3.0	33	0.09	11.0
3.0	38	0.088	12.7

not interact. Thus, for a stable flame to exist, the critical condition is given by Eq. (2).

$$L_{\rm int} = d_k \tag{2}$$

The OH* images at 5 kHz showed that the diameter of the OH*-pocket (d_k) created by each NRP discharge is between 3–5 mm. Table 1 shows the residence time (ms) for each OH*-pocket to travel 3 mm (minimum diameter of OH*-pocket). The residence time was converted to evaluate the minimum frequency required for the OH*-pockets to merge at each velocity. It was observed that the OH*-pockets production required for a stable flame is more than 5 kHz and close to 10 kHz for the bulk velocities considered in this work. Therefore, a change in flame structure and stability is observed when the NRP frequency is increased from 5 kHz to 10 kHz, and there is no dependency on the frequency beyond 10 kHz for the flame stability.

An empirical correlation typically used in studying the blow-off limits with conventional stabilisers is based on the Damköhler number which can be written as [30,31]:

$$\frac{1}{\mathrm{Da}^*} = \left[\left(\frac{C_1}{C_2} \frac{15}{A} \right) \left(\frac{u_b}{d} \frac{v}{S_L^2} \right) \right]^{1/2} \tag{3}$$

In the above expression, C_1 , C_2 and A are constants, v is the kinematic viscosity, u_b is the bulk flow velocity, d is the characteristic

dimension of the flameholder, and S_L is the laminar flame speed. In the case of a flame stabilised by a plasma without a bluff body, the above correlation needs to be modified as no characteristic flameholder lengthscale exists.

The kernel diameter d_k in the vicinity of the electrodes can be assumed to be proportional to the laminar flame thickness given by $\delta = \nu/S_L$ [32]. From the condition defined in Eq. (2), the modified critical Damköhler number Da* close to the extinction limit for plasma-stabilised flames can be defined as:

$$Da^* = \frac{d_k}{L_{\text{int}}} = \frac{vf}{u_b S_L} \tag{4}$$

The critical Damköhler number Da* corresponding to extinction conditions is shown in Fig. 9 at different repetition frequencies. The values are calculated by considering S_L at the extinction equivalence ratio as in [33] and kinematic viscosity of air at 298 K. From the figure, it can be observed that Da* is in the range between 0.01-0.04 for bulk velocities in the range of 25 m/s to 35 m/s. The higher value of Da* at lower velocities indicates a better flame stabilisation at these operating points. As Da* is inversely proportional to the square of laminar flame speed (see Eq. (4)) calculated at extinction equivalence ratios, a higher value of Da* at a particular velocity indicates the possibility of flame stabilisation at a lower equivalence ratio. This is what is observed from the experimental results shown in Fig. 7, where a flame can be stabilised at a lower equivalence ratio at lower velocities. Similarly, the evolution of Da* with frequency indicates that one can stabilise a flame better at higher frequencies. This is indeed the case as the frequency increases from 5 kHz (see Fig. 3 at $u_b = 28$ m/s) to 10 kHz (see Fig. 4 at $u_b = 28$ m/s). However, increasing the frequency further to 15 kHz (see Fig. 5 at $u_b = 28$ m/s) does not contribute to an improved flame stabilisation as the repetition frequency has no effect once the OH*pockets are merged. However, even if this modified Da* takes the effect of frequency into account and relies on the observation of individual kernel merging as the pre-requisite for overall flame stability, the spread of values is large, and hence, it does not appear to be sufficient as a numerical correlation for using in other conditions.

As an alternative, the extinction Karlovitz stretch factor K can be estimated based on the correlation given by Adbel-Gayed and Bradley [34] for turbulent premixed flame extinction. The modified version of this correlation given in [35] can be written as:

$$K = 0.25 \left(\frac{u'}{S_L}\right)^2 \text{Re}_t^{-0.5}$$
 (5)

where u' is the root mean square velocity fluctuations and Re_t is the turbulent Reynolds number given by u'l/v, where l is the turbulent integral lengthscale. Here, the lengthscale is taken as 10% of the channel width considering the case of a fully developed pipe flow [36], and it is assumed independent of the bulk velocity. The former assumption is consistent with expectations from turbulent duct flow, while the latter is consistent with any high Reynolds number turbulent flow. The turbulent intensity is taken as $u'/u_b = 0.2$ based on the particle image velocimetry measurements (not shown here) and is insensitive to the bulk velocity.

The evolution of the stretch factor K at the extinction condition with bulk velocity and repetition frequency is shown in Fig. 10. As the frequency is increased beyond $5\,\mathrm{kHz}$, the stretch factors for higher frequencies collapse to a value of about 2.1 for all velocities studied. Despite the uncertainty in the evaluation of K due to the use of an assumed integral lengthscale rather than a measured one, the critical K here seems to be similar to the critical K for premixed flame propagation, which was about 2 in Bradley and co-workers' experiments [35]. The spread of the experimental data in terms of K is not too large, suggesting that the Karlovitz number could offer a way to predict the stability limits of such plasma stabilisation systems for other fuels, mixtures and turbulence levels. It also suggests that the overall continuous flame sheet establishment in plasma-stabilised turbulent

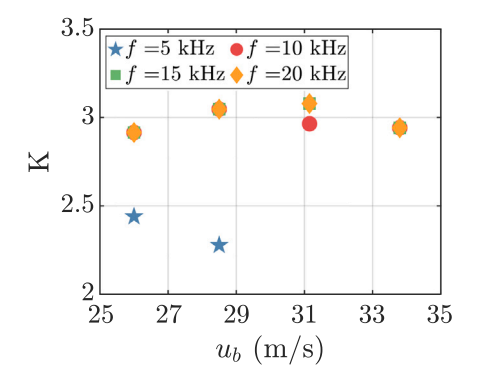


Fig. 10. Evolution of the Karlovitz stretch factor K with bulk velocity u_b and repetition frequency f. (For interpretation of the references to colour in this figure legend, the reader is referred to the web version of this article.)

premixed flames is more akin to turbulent flame ignition or extinction (which is what the K was originally conceived for) than conventional flameholder stabilisation by recirculation zones. More work on this is needed in the future.

5. Conclusions

This work discussed the potential of nanosecond repetitively pulsed plasma discharges to stabilise turbulent premixed flames in the absence of conventional stabilisers such as swirlers or bluff bodies.

Experiments were carried out in a square-cross-section combustor with a turbulent flow of premixed methane and air by systematically varying the plasma repetition frequency and energy. High-speed OH* chemiluminescence imaging showed that the OH*-pockets created by the spark are convected downstream by the bulk flow. At low velocities, these OH*-pockets merge together to form a continuous flame, but beyond a certain velocity, the OH*-pockets do not grow. It was found that a critical velocity exists for a particular plasma repetition frequency beyond which the OH*-pockets cannot merge to stabilise a flame. This condition was defined as the extinction limit, which was quantified at different repetition frequencies and energy levels and compared with that of a flame stabilised by a V-gutter bluff body. It was seen that at certain operating conditions, plasma-stabilised flames have similar stability limits to that of bluff body-stabilised flames. Within the limited range studied, the pulse energy does not appear to have a large effect on the stability limit. An analysis of the flame stabilisation limits with plasma was conducted, and it was found that the Karlovitz stretch factor K collapses the experimental data reasonably well, suggesting that K can be used to predict the critical condition for other fuels and operating conditions.

The present results offer further evidence that NRP discharges can be used to advantage in turbulent flame applications. In addition, they suggest that premixed flames at high speeds can be stabilised with NRP discharges in the absence of any other stabiliser, provided that the Karlovitz stretch factor remains above a critical value.

Novelty and significance statement

This research presents a novel way to stabilise turbulent premixed flames with plasma. While a majority of previous works on this topic have discussed flame stabilisation using a conventional flame stabiliser such as a swirler or bluff body and discussed the extension of the stability limits by plasma (i.e., plasma-assisted combustion), this work throws light on a flame stabilised only with nanosecond repetitively pulsed discharges, thus revealing the mechanism by which plasma can sustain a flame. In addition, it extends previous work on flame ignition with plasma discharges mostly carried out in laminar regimes towards flow systems at higher velocities and turbulence levels.

CRediT authorship contribution statement

Rohit Singh Pathania: Designed research, Performed research, Analysed data, Wrote the paper. Preethi Rajendram Soundararajan: Performed research, Analysed data, Wrote the paper, Prepared final draft. Epaminondas Mastorakos: Supervision, Secured funding, Prepared final draft.

Declaration of competing interest

The authors declare that they have no known competing financial interests or personal relationships that could have appeared to influence the work reported in this paper.

Acknowledgments

The authors are grateful for the discussions with Prof. Stewart Cant and Dr. Daniel Fredrich of the Cambridge University Engineering Department, which have greatly helped in this research work.

Appendix A. Supplementary data

Supplementary material related to this article can be found online at https://doi.org/10.1016/j.proci.2024.105722.

References

- [1] R.S. Pathania, A.W. Skiba, R. Ciardiello, E. Mastorakos, Blow-off mechanisms of turbulent premixed bluff-body stabilised flames operated with vapourised kerosene fuels, Proc. Combust. Inst. 38 (2021).
- [2] J. Kariuki, J.R. Dawson, E. Mastorakos, Measurements in turbulent premixed bluff body flames close to blow-off, Combust. Flame 159 (2012).
- [3] S. Chaudhuri, S. Kostka, M.W. Renfro, B.M. Cetegen, Blowoff dynamics of bluff body stabilized turbulent premixed flames, Combust. Flame 157 (2010).
- [4] S. Barbosa, G. Pilla, D.A. Lacoste, P. Scouflaire, S. Ducruix, C.O. Laux, D. Veynante, Influence of nanosecond repetitively pulsed discharges on the stability of a swirled propane/air burner representative of an aeronautical combustor, Philos. Trans. R. Soc. A: Math. Phys. Eng. Sci. 373 (2015).
- [5] G.T. Kim, C.S. Yoo, S.H. Chung, J. Park, Effects of non-thermal plasma on the lean blowout limits and CO/NOx emissions in swirl-stabilized turbulent lean-premixed flames of methane/air, Combust. Flame 212 (2020).
- [6] G. Pilla, D. Galley, D.A. Lacoste, F. Lacas, D. Veynante, C.O. Laux, Stabilization of a turbulent premixed flame using a nanosecond repetitively pulsed plasma, IEEE Trans. Plasma Sci. 34 (2006).
- [7] Y. Ju, W. Sun, Plasma assisted combustion: Dynamics and chemistry, Prog. Energy Combust. Sci. 48 (2015) 21–83.
- [8] A. Starikovskiy, Physics and chemistry of plasma-assisted combustion, Philos. Trans. R. Soc. A: Math. Phys. Eng. Sci. 373 (2015).
- [9] J. Gao, C. Kong, J. Zhu, A. Ehn, T. Hurtig, Y. Tang, S. Chen, M. Aldén, Z. Li, Visualization of instantaneous structure and dynamics of large-scale turbulent flames stabilized by a gliding arc discharge, Proc. Combust. Inst. 37 (2019).
- [10] J. Sun, Y. Tang, S. Li, Plasma-assisted stabilization of premixed swirl flames by gliding arc discharges, Proc. Combust. Inst. 38 (2021).
- [11] C.H. Kruger, C.O. Laux, L. Yu, D.M. Packan, L. Pierrot, Nonequilibrium discharges in air and nitrogen plasmas at atmospheric pressure, Pure App. Chem. 74 (2002).
- [12] D.Z. Pai, D.A. Lacoste, C.O. Laux, Transitions between corona, glow, and spark regimes of nanosecond repetitively pulsed discharges in air at atmospheric pressure, J. Appl. Phys. 107 (2010).
- [13] D.A. Xu, M.N. Shneider, D.A. Lacoste, C.O. Laux, Thermal and hydrodynamic effects of nanosecond discharges in atmospheric pressure air, J. Phys. D: Appl. Phys. 47 (2014).
- [14] S. Adams, J. Miles, T. Ombrello, R. Brayfield, J. Lefkowitz, The effect of inter-pulse coupling on gas temperature in nanosecond-pulsed high-frequency discharges, J. Phys. D: Appl. Phys. 52 (2019).
- [15] G. Vignat, N. Minesi, P. Rajendram Soundararajan, D. Durox, A. Renaud, V. Blanchard, C.O. Laux, S. Candel, Improvement of lean blow out performance of spray and premixed swirled flames using nanosecond repetitively pulsed discharges, Proc. Combust. Inst. 38 (2021).
- [16] V.P. Blanchard, P. Scouflaire, C.O. Laux, S. Ducruix, Combustion performance of plasma-stabilized lean flames in a gas turbine model combustor, App. Energy Combust. Sci. 15 (2023).
- [17] D.A. Lacoste, J.P. Moeck, C.O. Paschereit, C.O. Laux, Effect of plasma discharges on nitric oxide emissions in a premixed flame, J. Propul. Power 29 (3) (2013) 748-751
- [18] D.A. Lacoste, Flames with plasmas, Proc. Combust. Inst. 39 (2023).

- [19] Y. Bechane, B. Fiorina, Numerical analysis of turbulent flame enhancement by nanosecond repetitively pulsed plasma discharges, Proc. Combust. Inst. 39 (2023).
- [20] D.A. Lacoste, D.A. Xu, J.P. Moeck, C.O. Laux, Dynamic response of a weakly turbulent lean-premixed flame to nanosecond repetitively pulsed discharges, Proc. Combust. Inst. 34 (2013).
- [21] W. Kim, J. Snyder, J. Cohen, Plasma assisted combustor dynamics control, Proc. Combust. Inst. 35 (2015).
- [22] B. Dharmaputra, S. Shcherbanev, B. Schuermans, N. Noiray, Thermoacoustic stabilization of a sequential combustor with ultra-low-power nanosecond repetitively pulsed discharges, Combust. Flame 258 (2023).
- [23] I.N. Kosarev, N.L. Aleksandrov, S.V. Kindysheva, S.M. Starikovskaia, A.Y. Starikovskii, Kinetics of ignition of saturated hydrocarbons by nonequilibrium plasma: C2H6-to C5H12-containing mixtures, Combust. Flame 156 (2009).
- [24] T. Shiraishi, T. Urushihara, M. Gundersen, A trial of ignition innovation of gasoline engine by nanosecond pulsed low temperature plasma ignition, J. Phys. D: Appl. Phys. 42 (2009).
- [25] M.T. Nguyen, S.S. Shy, Y.R. Chen, B.L. Lin, S.Y. Huang, C.C. Liu, Conventional spark versus nanosecond repetitively pulsed discharge for a turbulence facilitated ignition phenomenon, Proc. Combust. Inst. 38 (2021).
- [26] C. Kong, Z. Li, M. Aldén, A. Ehn, Stabilization of a turbulent premixed flame by a plasma filament, Combust. Flame 208 (2019).
- [27] J.K. Lefkowitz, T. Ombrello, An exploration of inter-pulse coupling in nanosecond pulsed high frequency discharge ignition, Combust. Flame 180 (2017).

- [28] Y. Bechane, B. Fiorina, A numerical investigation of plasma-assisted ignition by a burst of nanosecond repetitively pulsed discharges, Combust. Flame 259 (2024).
- [29] R. Patel, J. van Oijen, S. Nijdam, N. Dam, On pulse-to-pulse coupling in low-temperature filamentary plasma-assisted ignition in methane-air flows, Plasma Sour. Sci. Tech. 32 (2023).
- [30] K. Radhakrishnan, J.B. Heywood, R.J. Tabaczynski, Premixed turbulent flame blowoff velocity correlation based on coherent structures in turbulent flows, Combust. Flame 42 (1981).
- [31] R.S. Pathania, A.W. Skiba, J.A.M. Sidey-Gibbons, E. Mastorakos, Lean blow-off scaling of turbulent premixed bluff-body flames of vaporized liquid fuels, J. Propuls. Power 37 (2021) 479–486.
- [32] J.R. Dawson, R.L. Gordon, J. Kariuki, E. Mastorakos, A.R. Masri, M. Juddoo, Visualization of blow-off events in bluff-body stabilized turbulent premixed flames, Proc. Combust. Inst. 33 (2011).
- [33] A. Massias, D. Diamantis, E. Mastorakos, D.A. Goussis, Global reduced mechanisms for methane and hydrogen combustion with nitric oxide formation constructed with CSP data, Combust. Theory Model. 3 (1999).
- [34] R. Abdel-Gayed, D. Bradley, Criteria for turbulent propagation limits of premixed flames, Combust. Flame 62 (1985).
- [35] D. Bradley, P.H. Gaskell, X.J. Gu, A. Sedaghat, Premixed flamelet modelling: Factors influencing the turbulent heat release rate source term and the turbulent burning velocity, Combust. Flame 143 (2005).
- [36] J.O. Hinze, Turbulence: An Introduction to Its Mechanism and Theory, McGraw-Hill Book Company, 1975.